Supplemental Figure captions

Supplemental Fig. 1. Interaction between MRLC3, the RXXT library and AATF. (A) FLAG-tagged MRLC3 co-precipitates with the non-phosphorylated RXXT library, but not its phosphorylated counterpart. FLAG-tagged MRLC3 was subcloned into pcDNA6 and expressed in HEK293T cells. *In vitro* pull down assays were performed using the streptavidin-immobilized ϕXRXXT (biotin-G-Z-G-Z-G-G-A-[L/I/F]-X-[R/K]-[Q/X]-X-T-X-[X no P]-X-X-A-K-K-K) and the ϕXRXXpT (biotin-G-Z-G-Z-G-G-A-[L/I/F]-X-[R/K]-[Q/X]-X-pT-X-[X no P]-X-X-A-K-K-K) peptide libraries as baits. While FLAG.MRLC3 readily co-precipitated with the ϕXRXXT library, we failed to recover FLAG.MRLC3 on the ϕXRXXpT library. **(B)** FLAG-tagged MRLC3 co-immunoprecipitates with V5-tagged AATF. V5-tagged AATF was co-expressed with FLAG-tagged MRLC3 in HEK293T cells. FLAG-tagged GFP served as a control. Lysates were incubated with anti FLAG M2-beads to immunoprecipitate FLAG.MRLC3. The precipitates were separated on SDS-PAGE and co-precipitating V5.AATF was subsequently detected by immunoblotting. **(C)** Doxorubicin treatment disrupts the interaction between FLAG-tagged MRLC3 and V5-tagged AATF. FLAG-tagged GFP served as a control. HEK293T cells were transfected with the indicated plasmids and either mock-treated or treated with 1 µM doxorubicin 60 min prior to lysis. Lysates were incubated with anti FLAG M2-beads to immunoprecipitate FLAG.MRLC3. The precipitates were separated on SDS-PAGE and co-precipitating V5.AATF was subsequently detected by immunoblotting.

Supplemental Fig. 2. Subcellular localization of AATF, Chk1 and MK2. (A) Indirect immunofluorescence was employed to determine the subcellular localization of AATF in resting cells. To verify the specificity of our antibody, we compared the staining patterns of the control cells with the cells in which AATF was depleted using RNAi. AATF showed specific cytoplasmic staining and unspecific nuclear background. **(B)** Indirect immunofluorescence was employed to verify the subcellular localization of the checkpoint kinase Chk1 60 min following UV-C-induced DNA damage (20 J/m^2). Chk1 resides in the nuclear

compartment in the absence or presence of UV-C-induced DNA damage (20 J/m^2) (middle panels). DAPI was used as a counterstain to provide a nuclear reference point. Immunoblotting with phospho-specific antibodies shows that Chk1 is activated in response to UV-C (top right panel). Total Chk1 staining served as a loading control (bottom right panels). **(C)** Indirect immunofluorescence was employed to verify the subcellular localization of the checkpoint kinase MK2 60 min following UV-C-induced DNA damage (20 J/m^2). DAPI was used as a counterstain to provide a nuclear reference point. In resting cells (top, middle) MK2 is predominately located within the nuclear compartment. Following UV-C irradiation MK2 is almost exclusively localized in the cytoplasm (bottom, middle). Immunoblotting with phospho-specific antibodies shows that MK2 is activated in response to UV-C (top right panel). Total MK2 staining served as a loading control (bottom right panels). **(D)** Cells were treated with 1 µM doxorubicin (dox) 60 min prior to fixation. Indirect immunofluorescence was used to monitor the subcellular localization of MK2. DAPI staining served as a counterstain to provide a nuclear reference point.

Supplemental Fig. 3. MK2 directly phosphorylates AATF *in vitro*. Active MK2 was incubated with recombinant 6xHis-tagged AATF 281-560 produced in the *E. coli* strain BL-21 in the presence of 10 µCi ^{32}P-γ-ATP. Recombinant MK2 was used at a concentration of 0.1 µM. Reactions were terminated after 5, 20 and 60 min by adding an equal volume of 0.5% phosphoric acid to the reaction, and the entire reaction was analyzed by 10% SDS PAGE followed by autoradiography. Additional reactions lacking MK2 were used as negative controls. MK2 readily phosphorylated AATF, while no significant ^{32}P incorporation could be detected in control reactions lacking MK2. Equal loading of 6xHis-tagged AATF was verified by coomassie staining of the SDS-PAGE gels.

Supplemental Fig. 4. MRLC3-binding stretches of AATF and myosin heavy chain share sequence and secondary structure similarities. (A) Clustal W alignment of AATF and myosin heavy chain (MHC) showing similarities between

the two peptide sequences. Specifically the basophilic residues appear to be located in similar positions within the amino acid sequences. **(B)** Secondary structure prediction of the MRLC3-binding aminoacid sequence of AATF. PSIPRED predictions show strong helical propensity in the AATF peptide, similar to the MRLC3-binding stretch within MHC (shown in Fig. 3D). C, coil; H, helix.

Supplemental Fig. 5. (A) MK2/3 knockout murine embryonic fibroblasts lack MK2 expression. *MK2*$^{wt/wt}$ and *MK2/3* double knockout (*MK2/3 DKO*) murine embryonic fibroblasts were lysed and immunoblotting with MK2-specific antibodies was performed. Tubulin staining of the PVDF Western blotting membranes served as a loading control. **(B)** RNAi-mediated knockdown efficiency. HCT116 cells were infected with lentiviruses expressing FLAG-tagged AATF **(B)** or FLAG-tagged MRLC3 **(C)**. Target cells were incubated with viral supernatants for 24 hrs in the presence of 8 µM polybrene. After three cycles of infection, cells were selected in puromycin for 48 hrs. These cells were subsequently superinfected with lentiviruses to express shRNAs targeting **(B)** AATF or **(C)** MRLC3. Following blasticidine selection cells were lysed and knockdown efficiency was assessed by SDS-PAGE. β-actin staining served as a loading control. **(D)** Overexpression of AATF leads to enhanced stability of DNA damage-induced cell cycle checkpoint. p53 proficient and p53-deficient HCT 116 cells were transduced to express either wildtype AATF or AATF-specific shRNA. 2h after application of genotoxic stress - UV-C (40J/m^2), camptothecin (cam) (10µM) or doxorubicin (dox) (1µM), cells were treated with nocodazole to arrest cells escaping DNA damage-induced cell cycle checkpoints in mitosis. 30 hours following application of genotoxic agents, cells were harvested for phospho-histone H3 staining followed by FACS analysis. Error bars represent standard deviations, n=8. Asterisk indicates statistical significance.

Supplemental Fig. 6. RNAi-mediated AATF depletion promotes DNA damage-induced apoptosis in p53-proficient cells, while loss of MRLC3 promotes resistance against genotoxic stress in p53-proficient cells.

SW1573 and NCI-H460 cells (both p53-proficient), as well as NCI-H23 and NCI-H2122 cell lines (both p53-defective) were retrovirally transduced to express shRNAs targeting AATF (left panels) or MRLC3 (right panels). Luciferase shRNA expression served as a negative control. Cells were treated with 10 μM camptothecin, 1 μM doxorubicin or 40 J/m^2 UV. 24 hrs later cells were harvested and the percentage of apoptotic cells was assessed using flow cytometry. Asterisk indicates statistical significance, error bars represent standard deviations, n=14.

Supplemental Fig. 7. Overexpression of the $AATF^{TD}$ mutant does not affect the sensitivity of p53-deficient HCT116 cell to DNA damage. p53-deficient HCT116 cells were lentivirally transduced to express either wildtype AATF ($AATF^{WT}$), the non-phosphorylatable AATF Thr-366 to Ala ($AATF^{TA}$) or the phospho-mimicking AATF Thr-366 to Asp ($AATF^{TD}$) mutant. Cells were left untreated or exposed to UV-C (40J/m^2), camptothecin (cam) (10μM) or doxorubicin (dox) (1 μM) and harvested for FACS-based quantification of apoptotic cells using a cleaved caspase-3 antibody 24 hrs later. Error bars represent standard deviations, n=11.

Supplemental Materials and Methods

Checkpoint kinase phospho-motif binding screen

An oriented phospho-threonine peptide library biased toward the motifs for Chk1 and MK2, and its non-phosphorylated counterpart were constructed as follows: biotin-G-Z-G-Z-G-G-A-[L/I/F]-X-[R/K]-[Q/X]-X-pT-X-[X no P]-X-X-A-K-K-K and biotin-G-Z-G-Z-G-G-A-[L/I/F]-X-[R/K]-[Q/X]-X-T-X-[X no P]-X-X-A-K-K-K where pT denotes phospho-Thr, Z indicates aminohexanoic acid, X denotes all amino acids except C for technical reasons. Streptavidin beads were incubated with a ten-fold molar excess of each biotinylated library in 50 mM Tris/HCl (pH7.6), 150 mM NaCl, 0.5% NP-40, 1 mM EDTA, 2 mM DTT and washed with the same buffer to remove unbound peptide. The bead-immobilized libraries were added to 10 µL of an *in vitro* translated ^{35}S-labeled protein pool in 150 µL binding buffer (50 mM Tris (pH7.6), 150 mM NaCl, 0.5% NP-40, 1 mM EDTA, 2 mM DTT). A mouse cDNA library with 100 plasmids per pool was *in vitro* transcribed, translated and radiolabeled by ProteoLink *in vitro* expression cloning system (Promega), giving ~30 radiolabeled proteins per pool. After incubation at 4ºC for 3 hours, beads were washed with binding buffer prior to SDS-PAGE and autoradiography. Pools containing positively scoring clones were progressively subdivided and re-screened for phospho-dependent regulation of binding until single clones were isolated and identified by DNA sequencing.

Two-hybrid screening

Yeast two-hybrid screening was performed with the ProQuest system (GIBCO) according to the manufacturer's protocol. As bait, MRLC3 was subcloned into pDBLeu. A ProQuest human kidney cDNA library was generated and used to transform the bait-containing yeast strain MaV203. Among more than 5 x 10^7 independent clones, 45 clones were selected on plates containing 25 mM 3-aminotriazole and lacking leucine, tryptophan, and histidine. Clones were tested for β-galactosidase activity and URA3 expression. Among 31 clones passing re-evaluation experiments 5 represented AATF.

Nano-LC ESI-MS/MS

Gel pieces were washed with 100mMTEAB/EtOH (50% v/v), dehydrated with acetonitrile, rehydrated with 100mM TEAB containing 0.5µg LysC (Wako) and incubated 4h at 37°C. Peptides were extracted with two gel-volumes of 0.1%TFA/60% acetonitrile and volume was reduced to 1/10 by vacuum centrifugation followed by elution with 0.1%TFA/80% acetonitrile. Enrichment of phosphopeptides by IMAC was done as described (Ficarro et al., 2009). Experiments were performed on a LTQ Orbitrap Discovery coupled to a Proxeon EASY-nLC II nano-LC system (Thermo). Peptides were detected in the Orbitrap at 30,000 resolution in the mass-to-charge range 300-2000 (MS). Calibration was performed using the ion signal of $(Si(CH_3)_2O)_6H$ at m/z 445.120025 as a lock mass. For LC-MS/MS analysis, up to four HCD and CID spectra (MS2) were acquired following each scan. When a neutral loss of phosphoric acid was detected, MS3 spectra were acquired in the linear ion trap to determine the peptide sequence. Aliquots of the sample were separated on a 10 cm, 75 µm reversed phase column (Proxeon). Gradient elution was performed from 10 to 30% acetonitrile within 80 minutes at a flow rate of 200 nl/min.

Peptide identification

Mascot 2.2 was used for protein identification. For intact peptide masses 10 ppm mass tolerance was allowed and 0.8 Da for CID fragment ions detected in the linear ion trap. Data were searched using the Swissprot and methionine oxidation and serine, threonine and tyrosine phosphorylation as variable modifications. Results were filtered to obtain only rank 1 peptides of high confidence with a Mascot ion score of ≥20 and peptide mass accuracy of ≤5ppm containing at least six amino acids.

Co-immunoprecipitation, nuclear preparation and Western blotting

Cells were washed with PBS, lysed in IP-buffer (1% Triton X-100; 20 mM Tris pH 7.5; 25mM NaCl; 50mM NaF; 15mM $Na_4P_2O_7$; 1mM EDTA; 0.25mM PMSF; 5 mMNa_3VO_4) on ice for 15 min and centrifuged (14.000rpm, 4°C, 15min).

Supernatants were incubated for 1 hr at 4°C with peptide library or peptides that were bound to streptavidin-beads or with anti FLAG antibody covalently coupled to agarose beads (Sigma). Precipitates were washed and bound proteins resolved on SDS-PAGE and visualized by immunoblotting.
For nuclear separation HCT116 cells or MEFs were lysed in 100µl hypotonic buffer (10mM HEPES, 1.5mM $MgCl_2$, 10mM KCl, 0.05% NP40, pH 7.9) and nuclear/cytoplasmic fractions were isolated as described before (Reinhardt et al.).

Immunofluorescence
Cells were fixed for 10 min in 4% PFA, incubated for 30 min in blocking solution (5% BSA, 0.1% Triton X-100) and subsequently incubated with primary and secondary antibodies. After washing, cells were mounted in Prolong Gold antifade (Invitrogen) and subjected to microscopy on an Axiovert 200M microscope equipped with a CCD camera (Zeiss). Fluorescence intensity of nuclear vs. cytoplasmic AATF-signal in randomly chosen high power fields of 30 cells per experiment was determined using Fiji image processing software.

FACS
Cells were washed in ice-cold PBS, trypsinized and fixed in 100% methanol at −20°C over night, blocked with 2% BSA in PBS, and incubated with primary antibody for 3 hrs. After washing, cells were incubated with Alexa-488-conjugated secondary antibodies (Molecular Probes, diluted 1:50) for 2 hr at room temperature, washed and resuspended in PBS containing 50µg/ml PI prior to analysis on a Beckman Gallios flow cytometer.

Kinase assay
For the *in vitro* kinase assay His.AATF 281-560 was expressed in BL-21 E. coli and purified using Ni-NTA (Qiagen). For mass spec FLAG.AATF was expressed in HEK293T cells and immunoprecipitated using anti FLAG antibody covalently coupled to agarose beads, c.f. section *Coimmunoprecipitation*. Kinase assays

were performed in identical 30 µl reactions containing 20 mM HEPES (pH 7.5), 10 mM $MgCl_2$, 3 mM β-mercaptoethanol, 100 µg/ml BSA, 50 µM ATP, 10 µCi ^{32}P-γ-ATP, and ~10 µM His.AATF 281-560 or FLAG.AATF, respectively at 30°C. Recombinant MK2 (Millipore) was used at a concentration of 0.1 µM. Reactions were terminated by adding an equal volume of 0.5% phosphoric acid, and the entire reaction was analyzed by 10% SDS PAGE. Phosphorstorage plates were imaged on the Typhoon Imager (GE). For mass spectrometry, the gels were stained using colloidal coommasie blue and the respective bands were excised manually.

Chromatin immunoprecipitation

$2x10^7$ UV-treated and untreated cells were crosslinked with 1% formaldehyde (Merck) for 10 minutes at RT. Crosslinking was quenched by addition of cold PBS. Cells were scraped into 50ml PBS containing protease inhibitors (PMSF and Aprotinin) and pelleted 5 min at 300 g at 4 °C. Cells were lysed and the lysate sonicated to a DNA fragment length of approx. 1kB. Lysate was cleared with CL-4B-200 beads (Sigma) and 2µg anti-AATF antibody (Abnova) was added for immunoprecipitation overnight. 60µl pre-blocked Gamma Binding G sepharose beads (GE health care) were added for one hour at 4 °C with rotation. After washing, beads were eluted in 500µl buffer. The eluate was incubated at 65°C overnight to reverse crosslinking, followed by proteinase K (Roche) digestion and DNA recovery using the PCR purification kit (Qiagen). DNA was eluted in 50µl H_2O and 4µl of the eluate was used per well as the template for real time PCR using a Sybr Green-based master mix (Applied Biosystems). p53 binding motifs upstream of Exon1 of each gene were identified using p53MH (Hoh et al., 2002). Primers for amplifying promoter DNA are at less than 1kB distance from the identified p53 binding sites. Primer sequences for promoter DNA amplification are as follows: mPUMA-forward 5'-GGG GTC AGC CTT TAG TGT AGT G-3', mPUMA-reverse: 5'-GAC AGT GAC AAC CCA AAA CGT A-3', mCDKN1a-forward: 5'-ATG GAG ACA GAG ACC CCA GAT A-3', mCDKN1a-reverse: 5'-ACA AAA GCA TCC TTC ACC TGA T-3', mBAX-forward: 5'-TTG

GAG CAA TCT CTT ATA GTG CAG-3', mBAX-reverse: 5'-AGC ACT AAG GAG GTT AAA GCA GAA-3', mBAK1-forward: 5'-TCA TTT TTC CTA GGC AGG ACA T-3', mBAK1-reverse: 5'-GGA ACT GAA GCA CAG AGA GGT T-3', mGADD45α-forward: 5'-ATT CTC ACA ACC AAC CAA AAC C-3', mGADD45α-reverse: 5'-TTC TGG TTG TGG ACA TCT TTT G-3', mRPRM-forward: 5'- GTC ACC TAC CAG CCT AAA AGA GAA-3', mRPRM-reverse: 5'- CTT CCT AAT GGC ACA CAC TTA CAC-3'

Xenograft model

For tumor regression assays, HCT116 cells were stably transfected with the indicated constructs. A total of 10^6 cells in 0.1 ml of PBS were injected subcutaneously into the flanks of *Ncr*$^{nu/nu}$ mice. Upon tumor formation, mice were treated with doxorubicin (5 mg/kg, i.p., 2x/wk), monitored for the indicated time and sacrificed. Tumor diameter was measured daily and volumes calculated as described earlier (Jiang et al., 2009). Experiments were performed in quadruplicate, and data plotted as sample means with error bars showing standard deviation. Experiments were approved by the committee of animal care of the University of Cologne.

Structural modeling

MRLC3-binding segments of myosin heavy chain and AATF (residues 351-380) were aligned using ClustalW. Secondary structure predictions were performed on the MRLC3-binding segment of AATF using PSIPRED (McGuffin et al., 2000) and JNET (Cuff and Barton, 1999). Images of the MRLC3-myosin heavy chain complex (PDB code 2OS8) were created using the PyMOL Molecular Graphics System, Version 1.2, LLC). Electrostatic calculations were performed using CHARMM (Miller et al., 2008).

SNP-arrays

The NSCLC cell lines in this study have been collected from commercial suppliers and cultured in RPMI media as described previously (Sos et al., 2009).

Genomic DNA was hybridized to Affymetrix 6.0 SNP arrays following manufacturer's instructions. After segmentation the data was visualized in the integrated genome viewer (IGV).

Human Tissues and Immunohistochemistry

All tumor samples stem from the CIO Biobank at the Institute of Pathology, University of Bonn and Cologne, Germany. All tumors were clinically and pathologically identified as being the primary and only neoplastic lesion. Tissue microarrays sections were stained and evaluated as previously described (Heukamp et al., 2006; Zimmer et al., 2008). Staining intensities were individually evaluated by two independent observers using a four-tier scoring system as described before. For AATF nuclear and cytoplasmic staining was evaluated respectively: 0 no or undefined background, 1 weak, 2 distinct and of moderate intensitiy, 3 strong and complete staining. The vast majority of p53 mutations stabilize the mutant protein (Bartek et al. 1990; Iggo et al. 1990). Immunohistochemical detection of gross overexpression is suitable to identify most of the mutations. Statistical analysis was performed using Fisher's exact test, with all P-values being two-sided and considered significant when $P < 0.01$.

Integrated genomic analysis of AATF in primary neuroblastoma

Tumor samples of 164 neuroblastoma patients (stage 1, n=32; stage 2, n=25; stage 3, n=30; stage 4, n=50; stage 4S, n=27) were examined by both gene expression microarray and array-based comparative genomic hybridization (aCGH) analysis. *MYCN* amplification was detected by FISH in 26 samples, while it was absent in 132 samples (not determined, n=2). All patients were registered in the respective clinical trial of the Gesellschaft für Pädiatrische Onkologie (GPOH) with informed consent. All samples were obtained at diagnosis and prior to cytotoxic treatment. Each tumor sample was reviewed by a pathologist to ensure a minimal tumor content of 60%. Gene expression profiles were generated using a 44K oligonucleotide microarray (Agilent Technologies, Santa Clara, CA, USA). In brief, 1 µg of total tumor RNA was linearly amplified and labeled with Cy3 using Agilent's one-color Quick Amp Labeling Kit

following the instructions of the protocol. After hybridization, washing and scanning, resulting TIFF-images were processed using Agilent's Feature Extraction software Version 9.5.1. Gene expression data were normalized using quantile normalization. The gene *AATF* was represented by two probes, *UKv4_A_23_P89460* and *UKv4_A_24_P262395*, referred to as probe 1 and probe 2, respectively. All gene expression data are available through ArrayExpress (http://www.ebi.ac.uk/microarray-as/ae; Accession: E-MTAB-179). High-resolution aCGH analysis was performed using either Agilent's 44K (n=80) or 105K (n=84) oligonucleotide microarrays. Briefly, 2.5-5 µg genomic tumor and reference DNA were labelled and processed for each hybridization according to the manufacturers' recommendations. Arrays were scanned at 5 µm resolution using the Agilent G2567AA Scanner, and images were extracted by Feature Extraction 9.5 software. Raw aCGH data were processed by computing the ratio between the Cy3 and the Cy5 color channels for each probe. Then, the baseline was adjusted by setting the genome-wide average of the probe ratios to 2. Finally, copy number segements where derived from the raw copy numbers using circular binary segmentation (Olshen et al., 2004). To determine the optimal prognostic cut-off value of *AATF* expression levels, we performed a Kaplan-Meier scanning approach using log-rank statistics implemented in the R package survival. In brief, every expression value in the cohort is considered as a potential cut-off value. For each potential cut-off value, a log-rank statistic is calculated between the resulting survival curves. The statistic reaches a maximum at the optimal cut-off value. P-values were corrected for multiple testing. Pearson's correlation was applied to determine the association of copy number and expression values, and statistical significance was calculated using the correlation test as implemented in R.

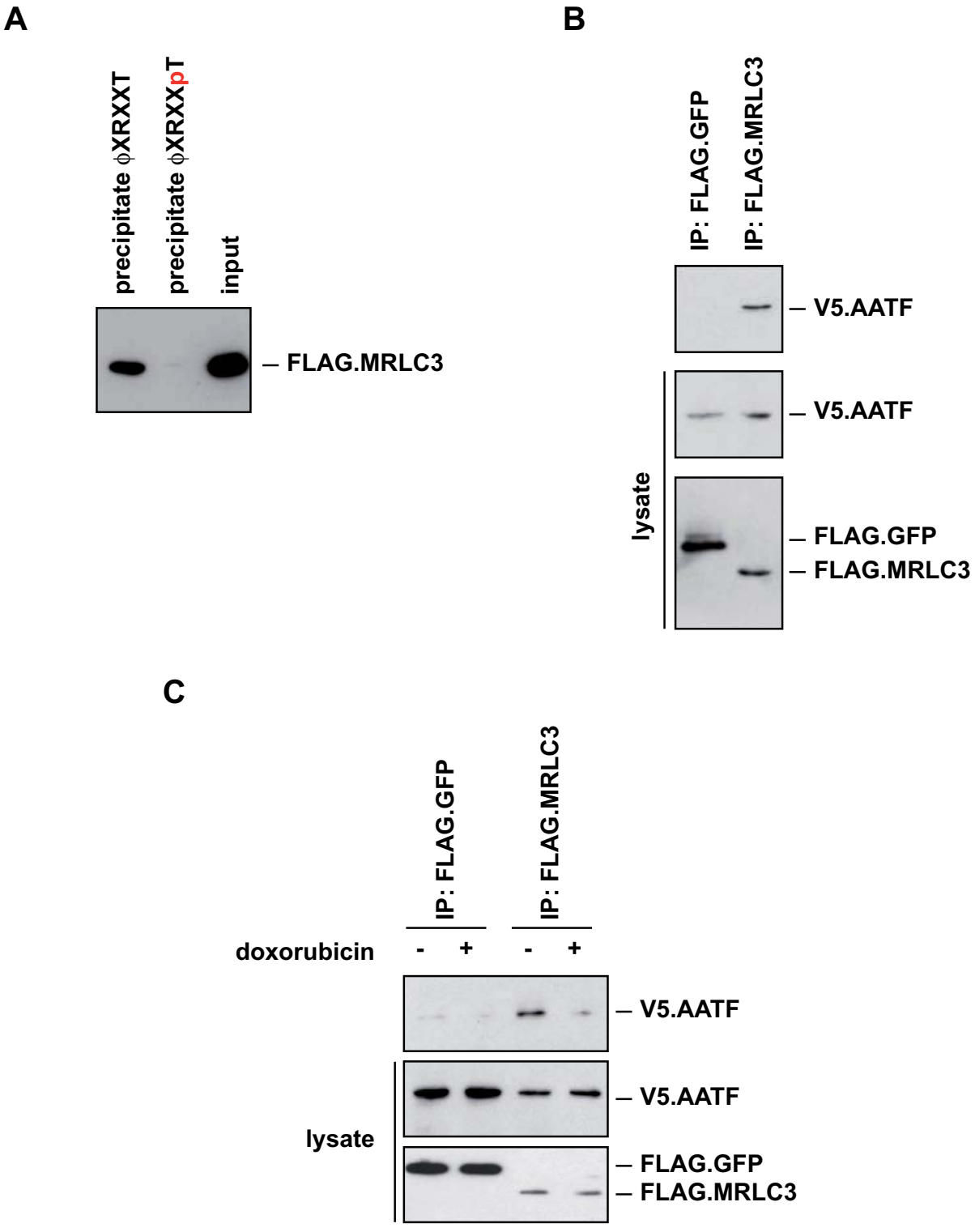
A
precipitate ϕXRXXT
precipitate ϕXRXXpT
input
– FLAG.MRLC3
B
IP: FLAG.GFP
IP: FLAG.MRLC3
– V5.AATF
– V5.AATF
lysate
– FLAG.GFP
– FLAG.MRLC3
C
IP: FLAG.GFP
IP: FLAG.MRLC3
doxorubicin
- + - +
– V5.AATF
– V5.AATF
lysate
– FLAG.GFP
– FLAG.MRLC3

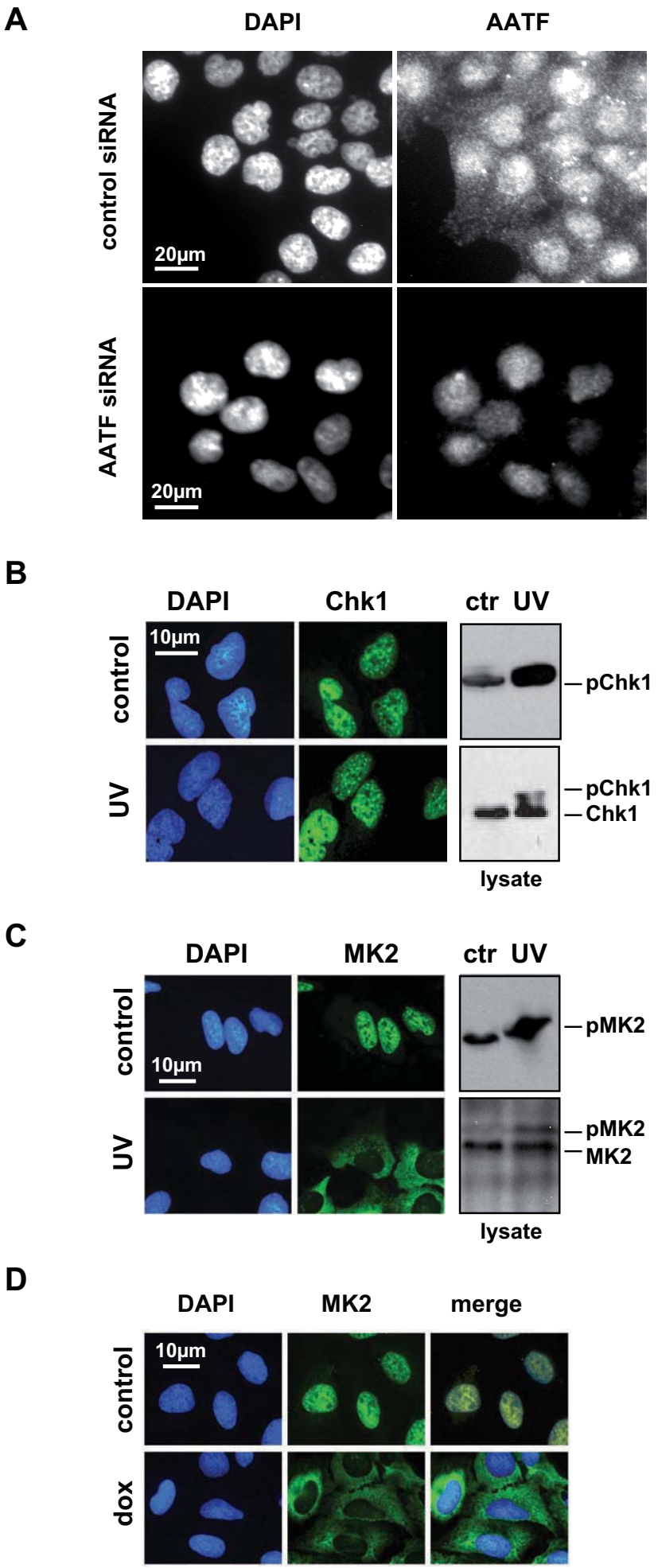
A
DAPI
AATF
control siRNA
AATF siRNA
20µm
20µm
B
DAPI
Chk1
ctr UV
control
UV
10µm
pChk1
pChk1
Chk1
lysate
C
DAPI
MK2
ctr UV
control
UV
10µm
pMK2
pMK2
MK2
lysate
D
DAPI
MK2
merge
control
dox
10µm

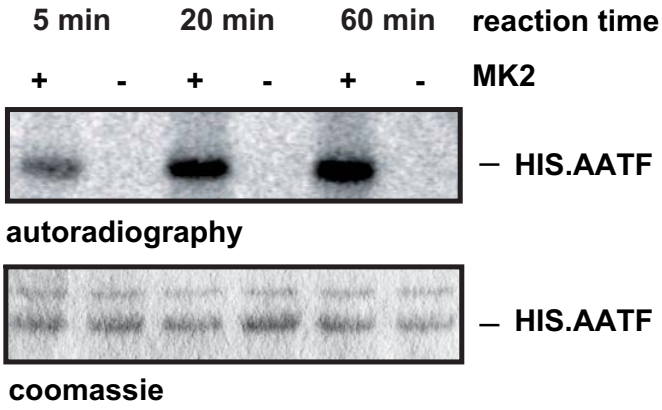
5 min
20 min
60 min
reaction time
+ - + - + -
MK2
– HIS.AATF
autoradiography
– HIS.AATF
coomassie

A

```
AATF        F----MAKRFADFTVYRNRTLQKWHDKTKLASGK
MHC         IGLSVIQRNIRKWLVLRNWQWWKLYAKVK----P
consensus   -glsvm-k----f-V-RN----K---K-Klasg-
```

B

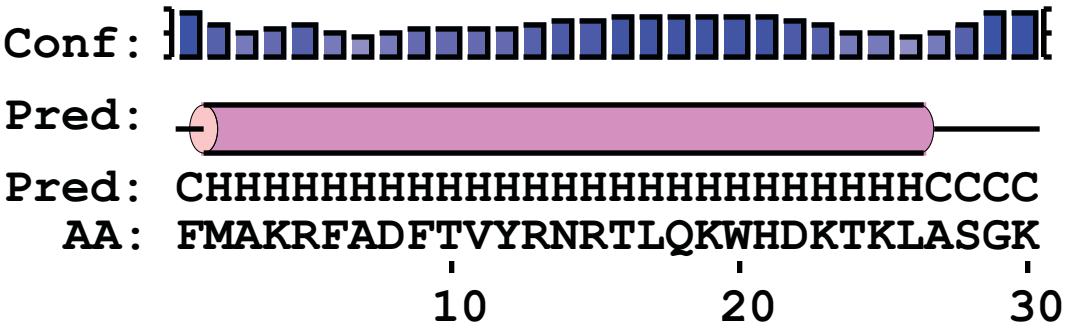

Legend:

= helix

= strand

= coil

Conf: = confidence of prediction

Pred: predicted secondary structure

AA: target sequence

Höpker et al., Supplemental Figure 5

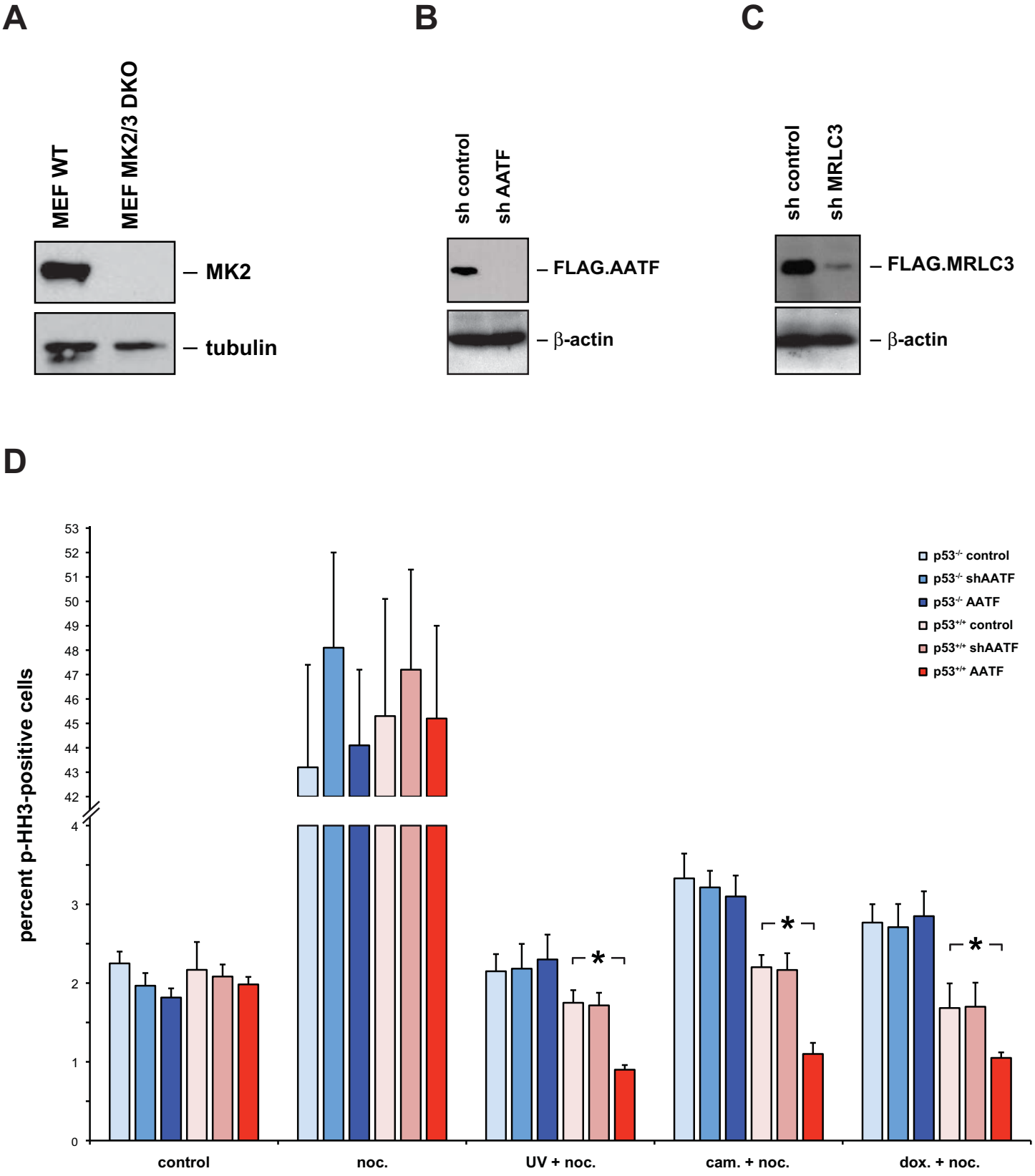

Höpker et al., Supplemental Figure 6

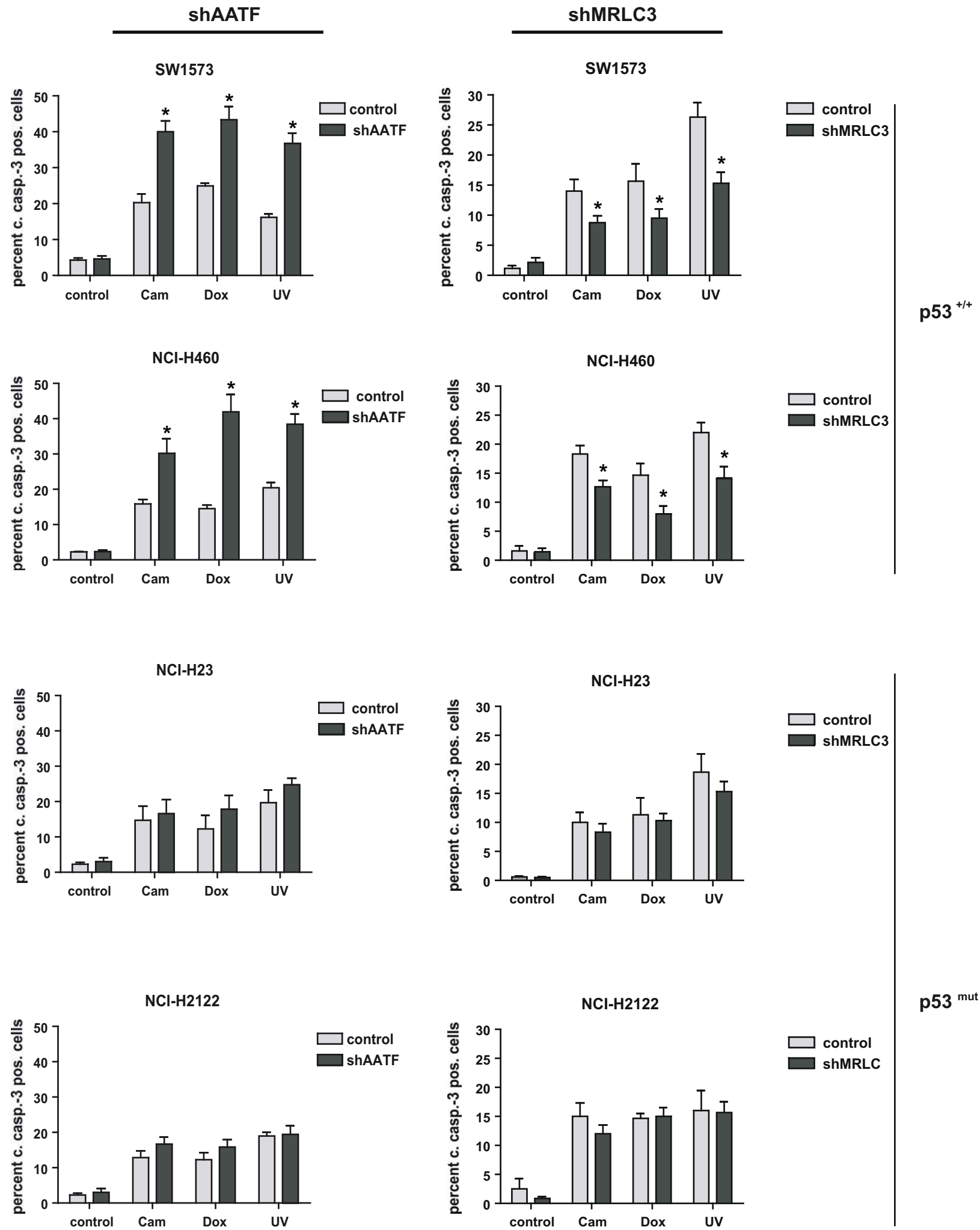

Höpker et al., Supplemental Figure 7